International Journal of Modern Physics B
Vol. 34, No. 9 (2020) 2050074 (20 pages)

DOI: 10.1142/S0217979220500745

Phase synchronization of memristive systems by using saturation gain method

Siyu Ma*, Ping Zhou†, Jun Ma*,† and Chunni Wang*,‡

*Department of Physics, Lanzhou University of Technology, Lanzhou 730050, P. R. China

†School of Science, Chongqing University of Posts and Telecommunications, Chongqing 430065, P. R. China

‡wangcn05@163.com; spiral911@126.com

Received 10 January 2020
Accepted 29 January 2020
Published 19 April 2020

A variety of electric components can be used to bridge connection to the nonlinear circuits, and continuous pumping and consumption of energy are critical for voltage balance between the output end. The realization and stability of synchronization are mainly dependent on the physical properties of coupling channel, which can be built by using different electric components such as resistor, capacitor, induction coil and even memristor. In this paper, a memristive nonlinear circuit developed from Chua circuit is presented for investigation of synchronization, and capacitor, induction coil are jointed with resistor for building artificial synapse which connects one output of two identical memristive circuits. The capacitance and inductance of the coupling channel are carefully adjusted with slight step increase to estimate the threshold of coupling intensity supporting complete synchronization. As a result, the saturation gain method applied to realize the synchronization between chaotic circuits and physical mechanism is presented.

Keywords: Memristor; synchronization; adaptive control; scale transformation; field coupling.

PACS number: 05.45.-a

1. Introduction

Chaotic systems present abundant dynamical properties than periodical oscillators, and the sampled signals can be approached by merging a variety of periodical signals with appropriate weights. On the other hand, chaotic signals can be tamed to produce certain periodical signals by applying effective schemes on the chaotic

‡Corresponding author.

systems.[1–3] It is believed that chaotic systems can be used for secure communication and image encryption.[4–6] As is well-known, the occurrence of chaos mainly depends on the nonlinearity and parameters region, which can be estimated by bifurcation analysis and calculating the Lyapunov exponent spectrum in numerical way. With respect to chaos control, most of the researchers claimed that chaos and hyperchaos can be suppressed or stabilized by using many effective schemes only when the chaotic systems are in controllability. In fact, chaos control seldom means that chaotic orbits should be regulated and guided for complete regularity. In fact, it is very important to explore and estimate the emergence of mixed modes and multiple modes in oscillation of nonlinear systems by applying periodical stimulus and parameters exciting[7–10] and the dynamical mechanism can be known by using the standard bifurcation analysis.[11–14]

Spatiotemporal systems, such as complex network, often contain a group of nodes and agents, which the local kinetics can often be described by maps and nonlinear oscillators. Due to self-organization and mutual coupling, the network often presents regular spatial patterns[15–18] or synchronous states[19–22] by selecting appropriate control conditions such as coupling intensity, time delay and topology connection.[23,24] On the other hand, local pacing[25,26] and heterogeneity[27,28] can generate continuous pulse and wave fronts and then the collective behaviors are regulated. Mutual coupling is important for building network with symmetrical network while unidirectional coupling is often used to connect a forward network[29,30] that reversed signal propagation is blocked. In particular, noise can be imposed on some memristive oscillators and synchronization can be stabilized even when no direct variable coupling is activated,[31] the potential mechanism could be noise stimulus which can enhance its initial dependence and two oscillators which can reach synchronization under coherence. In fact, variable coupling between the nonlinear oscillators results from the voltage coupling via resistor by applying the standard-scale transformation on physical variables.[32] For neurons and neural network, gap junction coupling[33–35] often explains the variable coupling as potentials coupling via electric synapse. However, some computational neuroscientists argue that chemical synapse coupling[36–38] could be the main bridge for connecting neurons and encoding signals. From the physical viewpoint,[39] electromagnetic field is built and field coupling is activated to propagate energy between neurons during the activation of chemical synapse by releasing neurotransmitter and calcium from the neurons.

Nonlinear oscillators provide feasible examples for synchronization approach by using Lyapunov stability theory and bifurcation analysis. On the other hand, nonlinear circuits present reliable experimental platform for estimating the controllability of synchronization realization. Joule heat effect should be considered when resistor is used to enable voltage coupling between chaotic circuits. Indeed, capacitive coupling generates time-varying electric field in the coupling capacitor,[40–42] which can pump energy from the two connected circuits, and appropriate capacitance

enables the balance between output voltage for reaching final synchronization. On other hand, inductive coupling induces time-varying magnetic field in the coupling induction coil,[43–46] which also is effective to pump energy from the circuits, and appropriate inductance for the coupling coil can balance the energy flow for reaching complete synchronization. One important question rises, what is the most suitable threshold for the coupling intensity and parameters value for the coupling components? From dynamical view, the coupled circuits can be mapped into dimensionless dynamical systems by applying scale transformation, and bifurcation analysis or stability analysis can be used to estimate the threshold for synchronization approach. However, when some of the parameters are unknown, this scheme becomes difficult because stability analysis requires exact knowing for the parameters.

The involvement of memristor[47–50] enhances the dynamics complexity in nonlinear circuits because mode transition can be induced by resetting initial value for the memristive variable such as magnetic flux even when all the parameters are fixed. Furthermore, memristor can also be effective to synchronize chaotic circuits and neurons.[51–53] In particular, the synchronization stability is also dependent on the initial setting for the memristive dynamical systems.[54–57] In this paper, linear resistor is connected with capacitor (and induction coil) to build a hybrid synapse for coupling the same output end of two identical memristive circuits developed from the Chua circuit. The capacitance (and inductance) of the coupling channel is carefully increased with constant step until complete synchronization is reached, and a Heaviside function is used to switch off the increase of coupling intensity. The coupling channel is built by connecting resistor and capacitor (and induction coil) in series (and/or in parallel), it is found that this kind of saturation gain method is effective to realize the complete synchronization between chaotic circuits when the coupling intensity is increased with step function before reaching the upper threshold.

2. Model and Scheme

Chua circuit[58–60] is the simplest nonlinear circuit, which the main electric components are two capacitors, one induction coil and one nonlinear diode. Memristor is a reliable electric component and its memductance is dependent on the magnetic flux or charges across it. In fact, the involvement of memristor in the nonlinear circuit just introduces time-varying but variable-dependent parameter, as a result, the dynamics of memristive system is dependent on the initial value and slight shift in the memristive variable will trigger distinct mode transition in oscillation even all the parameters are fixed. In this paper, a memristor and one negative resistor are used to replace the Chua diode in the original Chua circuit, and a constant voltage source is supplied to activate one branch of this new memristive circuit, which is presented in Fig. 1.

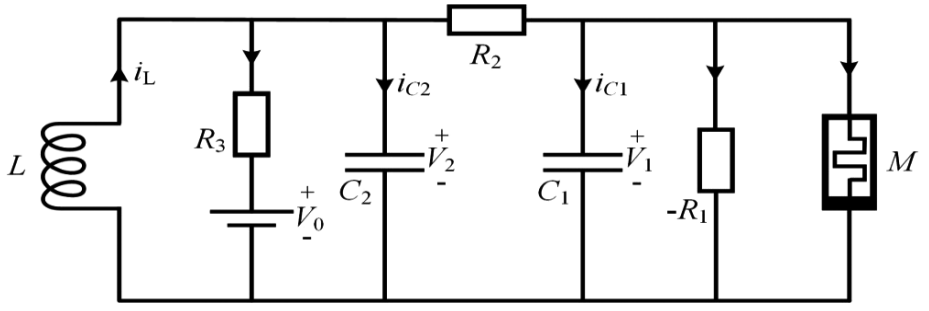

Fig. 1. Memristive Chua circuit. M is a magnetic flux-controlled memristor, $-R_1$ is negative resistor, C_1, C_2 are capacitors, L is induction coil, R_2, R_3 are resistors and V_0 is constant voltage source. The memductance of memristor is estimated by $W(\varphi) = \alpha + 3\beta\varphi^2$, α, β are intrinsic parameters of the memristor, φ is magnetic flux.

According to the physical Kirchhoff's law, the circuit equations for Fig. 1 can be obtained by

$$\begin{cases} C_1 \dfrac{dV_1}{dt} = \dfrac{V_2 - V_1}{R_2} + \dfrac{V_1}{R_1} - W(\varphi)V_1, \\ C_2 \dfrac{dV_2}{dt} = i_L - \dfrac{V_2 - V_1}{R_2} - \dfrac{V_2 - V_0}{R_3}, \\ L \dfrac{di_L}{dt} = -V_2, \\ \dfrac{d\phi}{dt} = V_1, \end{cases} \tag{1}$$

where V_1, V_2, i_L represent the output voltage from the capacitors C_1, C_2, and current across the induction coil L, respectively. For further nonlinear analysis, scale transformation is applied on the physical variables as follows:

$$\begin{cases} x = \dfrac{V_1}{V_0}, y = \dfrac{V_2}{V_0}, z = \dfrac{i_L R_2}{V_0}, \omega = \dfrac{\varphi}{V_0 R_2 C_2}, \alpha' = \alpha R_2, \beta' = 3\beta V_0^2 C_2^2 R_2^3, \\ a = \dfrac{C_2(R_2 - R_1)}{C_1 R_1}, b = \dfrac{C_2}{C_1}, c = \dfrac{R_2}{R_3}, d = \dfrac{C_2 R_2^2}{L}, \tau = \dfrac{t}{C_2 R_2}. \end{cases} \tag{2}$$

In addition, the dimensionless memristive system is estimated by

$$\begin{cases} \dot{x} = ax + b[y - (\alpha' + \beta'\omega^2)x], \\ \dot{y} = x - y + z - c(y - 1), \\ \dot{z} = -dy, \\ \dot{\omega} = x. \end{cases} \tag{3}$$

As is well-known, the capacitance of capacitor can be adjusted and enhanced when the dielectric medium is injected into the capacitor. Also, the inductance of the

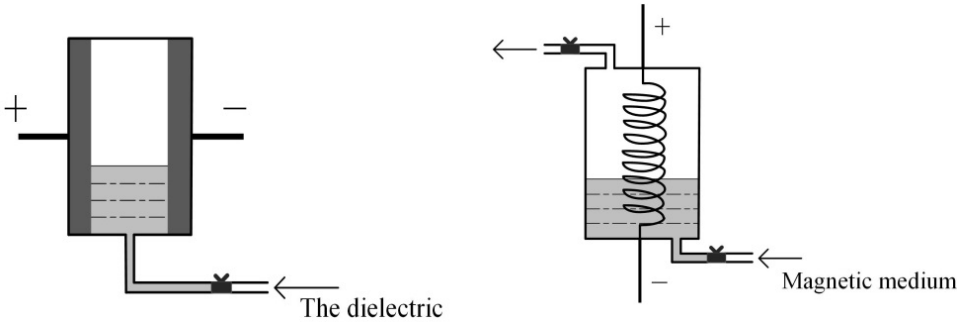

Fig. 2. Adjustment of capacitance of coupling capacitor (a) and inductance of induction coil and (b) for the coupling channel by pumping in (or out) the dielectric media and magnetic media of the coupling devices.

inductor can be modulated by injecting magnetic medium into the induction coil. Here, we suggest that the coupling capacitor and induction coil can be adjusted for selecting different capacitance and inductance values, and the experimental practice is shown in Fig. 2.

That is, the coupling capacitor, coupling induction coil can select time-varying capacitance $C(t)$, $L_x(t)$, respectively.

The time-varying and controllable capacitor and induction coil are used to connect one resistor R for building hybrid synapse for the coupling channel. There are four cases to be considered, the resistor connects the capacitor in series (case 1), resistor and capacitor are connected in parallel (case 2), the resistor connects the induction coil in series (case 3) and the resistor bridges the induction coil in parallel (case 4).

First, we consider the first case that the coupling channel is built by connecting the resistor with capacitor in series, and the circuit is plotted in Fig. 3.

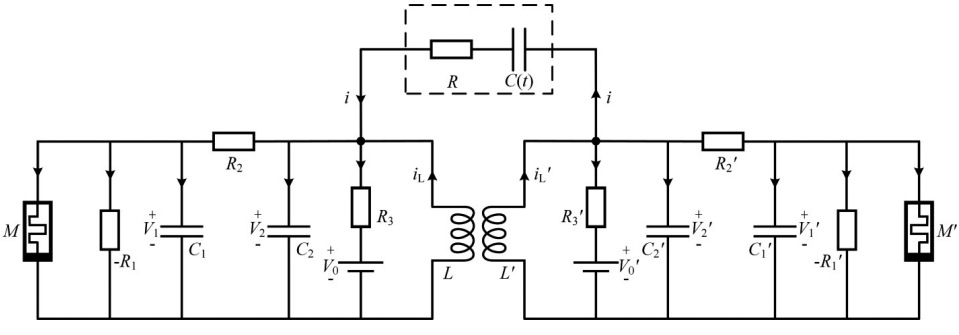

Fig. 3. Two memristive circuits are coupled by hybrid synapse, which is made of resistor R and controllable capacitor $C(t)$ in series. The time-varying current across the single coupling channel can be estimated by $i = Cd[V_2' - (V_2 + iR)]/dt$.

By applying the physical Kirchhoff's law, the coupled circuit can be estimated by the circuit equations as follows:

$$\begin{cases} C_1\dfrac{dV_1}{dt} = \dfrac{V_2 - V_1}{R_2} + \dfrac{V_1}{R_1} - W(\varphi)V_1, \\ C_2\dfrac{dV_2}{dt} = i_L - \dfrac{V_2 - V_1}{R_2} - \dfrac{V_2 - V_0}{R_3} + i, \\ L\dfrac{di_L}{dt} = -V_2, \\ \dfrac{d\varphi}{dt} = V_1, \\ C_1'\dfrac{dV_1'}{dt} = \dfrac{V_2' - V_1'}{R_2} + \dfrac{V_1'}{R_1} - W(\varphi')V_1', \\ C_2'\dfrac{dV_2'}{dt} = i_L' - \dfrac{V_2' - V_1'}{R_2} - \dfrac{V_2' - V_0'}{R_3} - i, \\ L'\dfrac{di_L'}{dt} = -V_2', \\ \dfrac{d\varphi'}{dt} = V_1', \\ CR\dfrac{di}{dt} = C\dfrac{d(V_2' - V_2)}{dt} - i. \end{cases} \tag{4}$$

Furthermore, the same scale transformation is applied on the variables for the coupled circuits. For simplicity, the two memristive circuits select the same electric components and parameters. $C_1 = C_1'$, $C_2 = C_2'$, $L = L'$, $V_0 = V_0'$, and the output variables for C_1, C_2, L are, respectively, mapped into x_1, y_1, z_1, while x_2, y_2, z_2 are used to represent the output variable for C_1', C_2', L'. Also, the feedback gains and channel current are replaced by

$$\xi = \frac{iR_2}{V_0}, \quad k_R = \frac{R_2}{R}, \quad k_C = \frac{2C + C_2}{C}. \tag{5}$$

In practical way, the capacitance of the coupling capacitor is adjusted by a linear step function, which can be approached with integer calculation (algorithm) as follows:

$$C(t) = C_0 + \mu_0 \ \mathrm{int}(t/T_0)H(|V_2 - V_2'| - \varepsilon), \tag{6}$$

where $H(\Theta)$ is the standard Heaviside function, e.g., $H(\Theta) = 1$ at $\Theta > 0$ and $H(\Theta) = 0$ at $\Theta < 0$. ε is an infinitesimal value about 10^{-5}. Int$(*)$ means integer calculation, t is time and T_0 is step period. For example, with an increase period T_0, the capacitance will show an increase with μ_0. C_0 is the beginning

value for the coupling capacitor. That is, after a step period T_0, the coupling capacitor increases its capacitance with $\Delta C = \mu_0$. When complete synchronization is approached, the coupling capacitor will fix the capacitance and the coupling channel is closed rapidly, as a result, the threshold for coupling intensity is detected.

In addition, the coupled circuits can be rewritten by the dimensionless dynamical systems as follows:

$$\begin{cases} \dot{x}_1 = ax_1 + b[y_1 - (1 + w_1^2)x_1], \\ \dot{y}_1 = x_1 - y_1 + z_1 - c(y_1 - 1) + \xi, \\ \dot{z}_1 = -dy_1, \\ \dot{\omega}_1 = x_1, \\ \dot{x}_2 = ax_2 + b[y_2 - (1 + w_2^2)x_2], \\ \dot{y}_2 = x_2 - y_2 + z_2 - c(y_2 - 1) - \xi, \\ \dot{z}_2 = -dy_2, \\ \dot{\omega}_2 = x_2, \\ \dot{\xi} = k_R[x_2 - x_1 + (y_1 - y_2)(1 + c) + z_2 - z_1 - k_C\xi]. \end{cases} \tag{7}$$

In fact, the coupled memrisitve circuits can present different forms when the coupling channel is connected to different output end, and the current across the coupling channel is also mapped to dimensionless term to adjust the corresponding variable of the dynamical systems. It is interesting to consider the second case that the resistor connects with the capacitor in series for opening the coupling channel, and the circuit is plotted in Fig. 4.

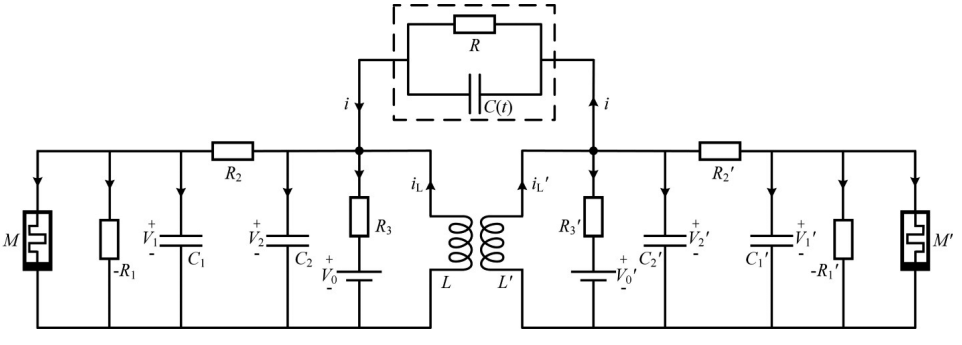

Fig. 4. Two memristive circuits are coupled by hybrid synapse, which is made of resistor R and controllable capacitor $C(t)$ in parallel. The time-varying current across the single coupling channel can be estimated by $i = Cd(V_2' - V_2)/dt + (V_2' - V_2)/R$.

According to the physical Kirchhoff's law for the coupled circuits shown in Fig. 4, the circuit equations can be obtained by

$$\begin{cases} C_1\dfrac{dV_1}{dt} = \dfrac{V_2 - V_1}{R_2} + \dfrac{V_1}{R_1} - W(\varphi)V_1, \\ C_2\dfrac{dV_2}{dt} = i_L - \dfrac{V_2 - V_1}{R_2} - \dfrac{V_2 - V_0}{R_3} + \left[\dfrac{V_2' - V_2}{R} + C\dfrac{d(V_2' - V_2)}{dt}\right], \\ L\dfrac{di_L}{dt} = -V_2, \\ \dfrac{d\varphi}{dt} = V_1, \\ C_1'\dfrac{dV_1'}{dt} = \dfrac{V_2' - V_1'}{R_2} + \dfrac{V_1'}{R_1} - W(\varphi')V_1', \\ C_2'\dfrac{dV_2'}{dt} = i_L' - \dfrac{V_2' - V_1'}{R_2} - \dfrac{V_2' - V_0''}{R_3} - \left[\dfrac{V_2' - V_2}{R} + C\dfrac{d(V_2' - V_2)}{dt}\right], \\ L\dfrac{di_L'}{dt} = -V_2', \\ \dfrac{d\varphi'}{dt} = V_1'. \end{cases} \tag{8}$$

The capacitance of the coupling capacitor is adjusted with the same step in Eq. (6) and the same parameters are selected to couple two identical memristive circuits. By applying the similar scale transformation, the coupled dynamical systems are estimated by

$$\begin{cases} \dot{x}_1 = \alpha x_1 + b[y_1 - (\alpha' + \beta' w_1^2)x_1], \\ \dot{y}_1 = [x_1 - y_1 + z_1 - c(y_1 - 1) + k_R(y_2 - y_1)] + \dfrac{1}{k_C}\{[x_2 - y_2 + z_2 - c(y_2 - 1) \\ \qquad - k_R(y_2 - y_1)] - [x_1 - y_1 + z_1 - c(y_1 - 1) + k_R(y_2 - y_1)]\}, \\ \dot{z}_1 = -dy_1, \\ \dot{\omega}_1 = x_1, \\ \dot{x}_2 = ax_2 + b[y_2 - (\alpha' + \beta' w_2^2)x_2], \\ \dot{y}_2 = [x_2 - y_2 + z_2 - c(y_2 - 1) - k_R(y_2 - y_1)] + \dfrac{1}{k_C}\{[x_1 - y_1 + z_1 - c(y_1 - 1) \\ \qquad + k_R(y_2 - y_1)] - [x_2 - y_2 + z_2 - c(y_2 - 1) - k_R(y_2 - y_1)]\}, \\ \dot{z}_2 = -dy_2, \\ \dot{\omega}_2 = x, \end{cases} \tag{9}$$

where the gains in Eq. (9) are calculated with the same definition in Eq. (5), as a result, the coupling intensity k_C can be tamed to find the threshold for synchronization. According to the criterion in Eqs. (6), the coupling gain k_C for the coupled dynamical systems in Eqs. (7)–(9) can also be adjusted with similar step function, where the capacitance is increased with constant step value in each interval period.

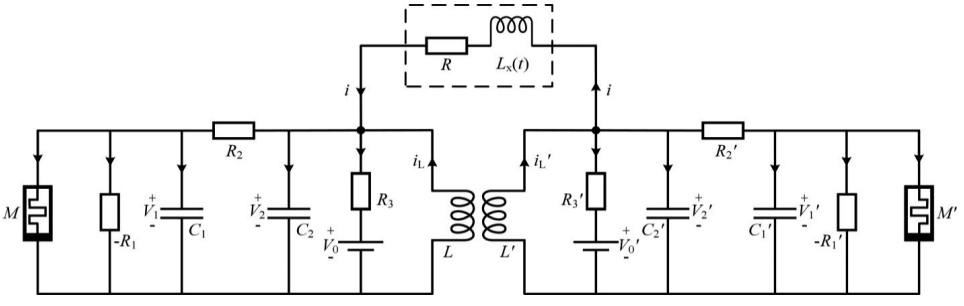

Fig. 5. Two memristive circuits are coupled by hybrid synapse, which is made of resistor R and controllable induction coil $L_x(t)$ in series. The time-varying current across the single coupling channel can be estimated by the requirement $L_x di/dt = V_2' - V_2 - iR$.

As mentioned above, induction coil is also effective to pump energy from the coupled nonlinear circuits, and thus the output voltage can be balanced for reaching complete or partial synchronization. In Fig. 5, the same resistor is connected to an induction coil in series, and the coupling channel is built for synchronization control.

By the way, the circuit equations for Fig. 5 can be approached to estimate the dependence and relation on the output variable as follows:

$$\begin{cases} C_1 \dfrac{dV_1}{dt} = \dfrac{V_2 - V_1}{R_2} + \dfrac{V_1}{R_1} - W(\phi)V_1, \\ C_2 \dfrac{dV_2}{dt} = i_L - \dfrac{V_2 - V_1}{R_2} - \dfrac{V_2 - V_0}{R_3} + i, \\ L \dfrac{di_L}{dt} = -V_2, \\ \dfrac{d\phi}{dt} = V_1, \\ C_1' \dfrac{dV_1'}{dt} = \dfrac{V_2' - V_1'}{R_2} + \dfrac{V_1'}{R_1} - W(\phi')V_1', \\ C_2' \dfrac{dV_2'}{dt} = i_L' - \dfrac{V_2' - V_1'}{R_2'} - \dfrac{V_2' - V_0'}{R_3'} - i, \\ L' \dfrac{di_L'}{dt} = -V_2', \\ \dfrac{d\phi'}{dt} = V_1', \\ L_x \dfrac{di}{dt} = V_2' - V_2 - iR. \end{cases} \tag{10}$$

By applying the similar scale transformation on the physical variables and parameters, dimensionless dynamical equations can be mapped from the coupled circuit equations. The induction current and feedback gains can be estimated by

$$\delta = \frac{iR_2}{V_0}, \quad k_R = \frac{R_2}{R}, \quad k_L = \frac{C_2 R_2^2}{L_x}. \tag{11}$$

In experimental viewpoint, the inductance of the coupling induction coil can also be adjusted with step increase as follows:

$$L_x(t) = L_0 + \mu_0 \ \mathrm{int}(t/T_0) H(|V_2 - V_2'| - \varepsilon). \tag{12}$$

As a result, the coupled circuits can be rewritten by the dimensionless dynamical equations as follows:

$$\begin{cases} \dot{x}_1 = ax_1 + b[y_1 - (\alpha' + \beta' w_1^2)x_1], \\ \dot{y}_1 = x_1 - y_1 + z_1 - c(y_1 - 1) + \delta, \\ \dot{z}_1 = -dy_1, \\ \dot{\omega}_1 = x_1, \\ \dot{x}_2 = ax_2 + b[y_2 - (\alpha' + \beta' w_2^2)x_2], \\ \dot{y}_2 = x_2 - y_2 + z_2 - c(y_2 - 1) - \delta, \\ \dot{z}_2 = -dy_2, \\ \dot{\omega}_2 = x_2, \\ \dot{\delta} = k_L \left(y_2 - y_1 - \dfrac{1}{k_R}\delta \right). \end{cases} \tag{13}$$

From dynamical viewpoint, the coupling and feedback gains k_L, k_R can be modulated to detect the region for reaching complete and/or phase synchronization. In addition, we also consider the case when the coupling channel is built by connecting the induction coil and resistor in parallel, and the circuits are plotted in Fig. 6.

From Fig. 6, the coupled circuits can be described by

$$\begin{cases} C_1 \dfrac{dV_1}{dt} = \dfrac{V_2 - V_1}{R_2} + \dfrac{V_1}{R_1} - W(\phi)V_1, \\ C_2 \dfrac{dV_2}{dt} = i_L - \dfrac{V_2 - V_1}{R_2} - \dfrac{V_2 - V_0}{R_3} + \left(\dfrac{V_2' - V_2}{R} + i \right), \\ L \dfrac{di_L}{dt} = -V_2, \\ \dfrac{d\phi}{dt} = V_1, \\ C_1' \dfrac{dV_1'}{dt} = \dfrac{V_2' - V_1'}{R_2} + \dfrac{V_1'}{R_1} - W(\phi')V_1', \\ C_2' \dfrac{dV_2'}{dt} = i_L' - \dfrac{V_2' - V_1'}{R_2'} - \dfrac{V_2' - V_0'}{R_3'} - \left(\dfrac{V_2' - V_2}{R} + i \right), \\ L' \dfrac{di_L'}{dt} = -V_2', \\ \dfrac{d\phi'}{dt} = V_1', \\ L_x \dfrac{di}{dt} = V_2' - V_2. \end{cases} \tag{14}$$

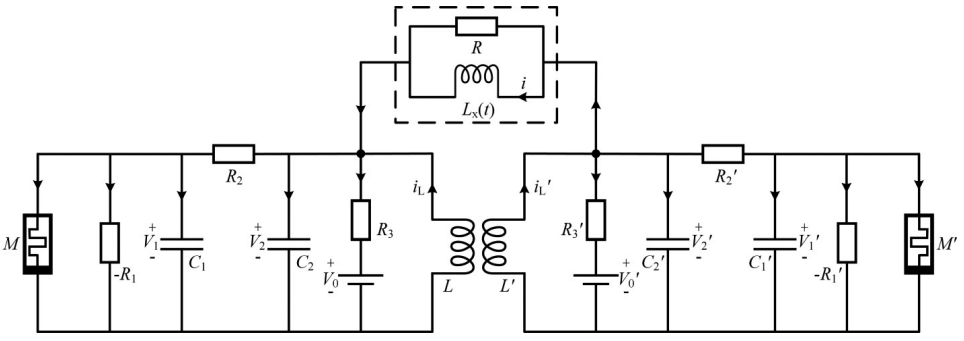

Fig. 6. Two memristive circuits are coupled by hybrid synapse, which is made of resistor R and controllable induction coil $L_x(t)$ in parallel. The time-varying current across the single coupling channel can be estimated by the requirement $L_x di/dt = V_2' - V_2 - iR$.

For further dynamical analysis and estimating synchronization stability, the same scale transformation on variables and parameters are applied, and the dimensionless dynamical systems are obtained by

$$\begin{cases} \dot{x}_1 = ax_1 + b[y_1 - (\alpha' + \beta' w_1^2)x_1], \\ \dot{y}_1 = x_1 - y_1 + z_1 - c(y_1 - 1) + [k_R(y_2 - y_1) + \delta], \\ \dot{z}_1 = -dy_1, \\ \dot{\omega}_1 = x_1, \\ \dot{x}_2 = ax_2 + b[y_2 - (\alpha' + \beta' w_2^2)x_2], \\ \dot{y}_2 = x_2 - y_2 + z_2 - c(y_2 - 1) - [k_R(y_2 - y_1) + \delta], \\ \dot{z}_2 = -dy_2, \\ \dot{\omega}_2 = x_2, \\ \dot{\delta} = k_L(y_2 - y_1). \end{cases} \tag{15}$$

In generic way, the error function is calculated to judge the synchronization stability when all the output variables are available.

$$\theta(e_x, e_y, e_z, e_w) = \sqrt{(x_1 - x_2)^2 + (y_1 - y_2)^2 + (z_1 - z_2)^2 + (w_1 - w_2)^2}. \tag{16}$$

In fact, when memristor is involved into the nonlinear circuit, its dynamics is much dependent on the initial setting for magnetic flux variable and the synchronization transition can be induced when slight difference is generated for the memristive variable. The dynamical mechanism is that slight diversity in the initial value for memeristive variable just induces mismatch in nonlinear parameter. Therefore, the two memristive circuits become nonidentical even when other constant parameters are the same; as a result, phase synchronization can be stabilized by modulating the coupling gain. The phase series can be calculated by applying the Hilbert transformation on the sampled time series for some output variables,

e.g., the output voltage.

$$\begin{cases} \hat{x}(t) = -\dfrac{1}{\pi} PV \displaystyle\int_{-\infty}^{\infty} \frac{x(\tau)}{t-\tau} d\tau, \\ \hat{x}'(t) = -\dfrac{1}{\pi} PV \displaystyle\int_{-\infty}^{\infty} \frac{x'(\tau)}{t-\tau} d\tau, \end{cases} \tag{17}$$

where PV denotes the principal value of the integral. In addition, the error for phase series is estimated by

$$\Delta\phi = \phi(t) - \phi'(t) = \arctan \frac{\hat{x}(t)}{x(t)} - \arctan \frac{\hat{x}'(t)}{x'(t)}. \tag{18}$$

3. Results and Discussion

In this section, the fourth-order Runge–Kutta algorithm is applied to find solutions for the dynamical equations with time step $h = 0.05$. The transient period for calculation is about 5000 time units, initial values for the two memristive systems are selected with (0.1, 0.1, 0.1, 0.1, 0.1, 0.3, 0.1, 0.1). The parameters are fixed at $a = -12.22$, $b = 10$, $c = 0.1$, $d = 14.286$, for simplicity, $\alpha' = 1$, $\beta' = 1$. In estimating the phase series, the time interval 0.5 is used to pick data from the sampled time series for the output variable. At first, we consider the case that the hybrid synapse is made of resistor connecting the capacitor in series, and the results are shown in Fig. 7.

It is found that the capacitance of the coupling capacitor is increased with constant step, and the two chaotic memristive systems reach intermittent phase

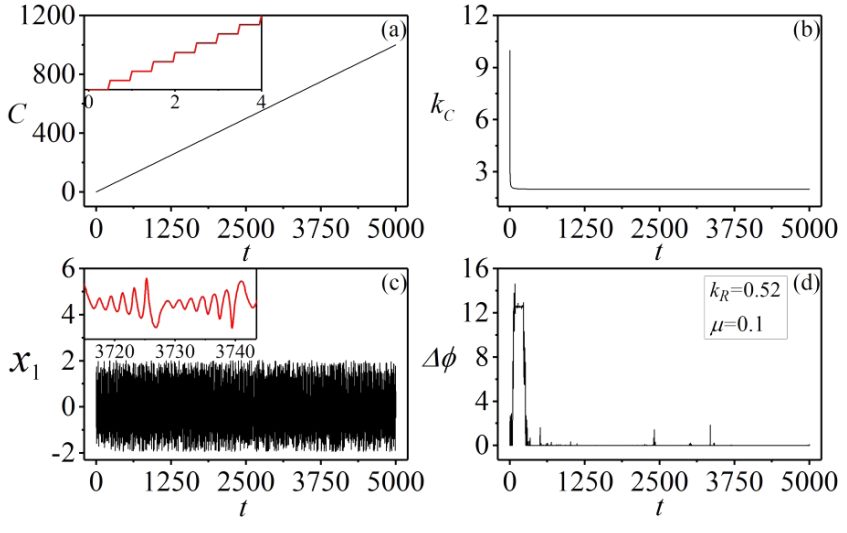

Fig. 7. (Color online) Synchronization approach by using saturation gain method. (a) Increasing the capacitance of coupling capacitor with step function; (b) regulation of the coupling gain; (c) sampled time series for variable x_1 and (d) evolution of phase error under field coupling. $k_R = 0.52$, $\mu_0 = 0.1$, and the coupling devices are connected in series.

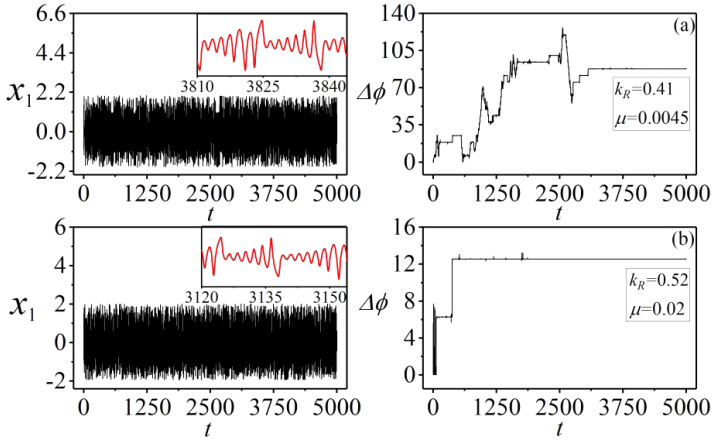

Fig. 8. (Color online) Synchronization approach by using saturation gain method. (a) Sampled time series for variable x_1 and evolution for phase error, $k_R = 0.41$, $\mu_0 = 0.0045$ and (b) sampled time series for variable x_1 and evolution for phase error, $k_R = 0.52$, $\mu_0 = 0.002$. The coupling devices are connected in parallel.

synchronization. By further increasing the intensity of voltage coupling via the resistor in the coupling channel, the transient period for reaching phase synchronization can be shorten greatly. Furthermore, it is interesting to discuss the case when the coupling channel is built by connecting the resistor and capacitor in parallel, and the results are shown in Fig. 8.

That is, with the increase of capacitance of the coupling capacitor, the two chaotic memristive systems show stable phase lock which is dependent on the intensity of voltage coupling k_R and step increase of the capacitance for the coupling capacitor. Extensive numerical investigations are carried out when the step increase for capacitance and coupling resistor is selected with another group of values, and the results are plotted in Fig. 9.

With further increase of the intensity of voltage coupling k_R and selecting larger step increase for the capacitance (μ_0), chaos in the two memristive systems is suppressed to present phase lock in periodical oscillators. Furthermore, the coupling resistor and capacitor are carefully adjusted to find phase synchronization, and the results are shown in Fig. 10.

As is well-known, nonlinear circuits can be tamed to produce spiking, bursting series and thus neural circuits are applied to simulate the neural activities. In Fig. 11, the output voltage and phase error are calculated by setting appropriate values for the coupling devices.

That is, the memristive systems are tamed to show spiking in the output voltage and phase lock occurs when the intensity for voltage coupling is selected with smaller value. On the other hand, the same scheme and algorithm is applied to discuss the case when the resistor is connected to the induction coil in series (and in parallel), respectively.

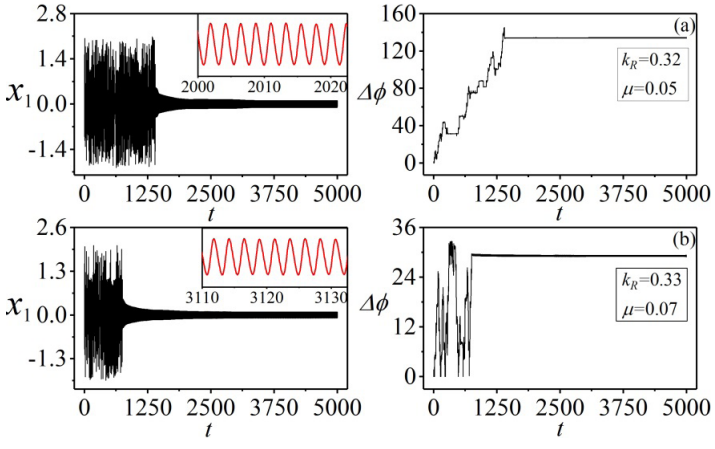

Fig. 9. (Color online) Synchronization approach by using saturation gain method. (a) Sampled time series for variable x_1 and evolution for phase error, $k_R = 0.32$, $\mu_0 = 0.05$ and (b) sampled time series for variable x_1 and evolution for phase error, $k_R = 0.33$, $\mu_0 = 0.07$. The coupling devices are connected in parallel.

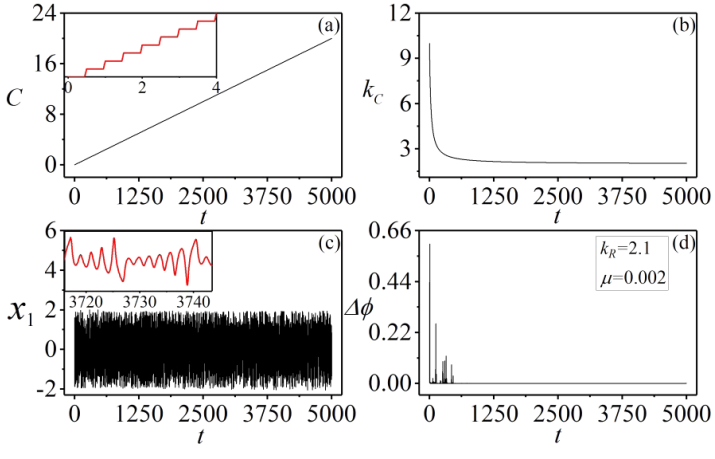

Fig. 10. (Color online) Synchronization approach by using saturation gain method. (a) Increasing the capacitance of coupling capacitor with step function; (b) regulation of the coupling gain; (c) sampled time series for variable x_1 and (d) evolution of phase error under field coupling. $k_R = 2.1$, $\mu_0 = 0.002$, and the coupling devices are connected in parallel.

It is found that the two memristive systems can reach the phase synchronization and the chaos is kept completely when hybrid synapse is used to activate the magnetic field coupling and voltage coupling synchronously. Furthermore, changing the intensity for voltage coupling and step increase for the capacitance, phase lock can be detected in Fig. 13.

That is, the two memristive systems step into transient phase lock and chaos is kept completely. Then coupling gain is carefully selected to detect phase lock when

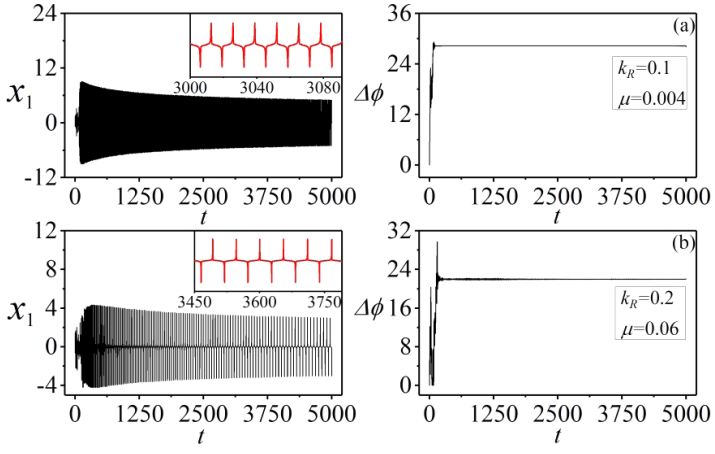

Fig. 11. (Color online) Synchronization approach by using saturation gain method. (a) Sampled time series for variable x_1 and evolution for phase error, $k_R = 0.1$, $\mu_0 = 0.004$ and (b) sampled time series for variable x_1 and evolution for phase error, $k_R = 0.2$, $\mu_0 = 0.06$. The coupling devices are connected in parallel.

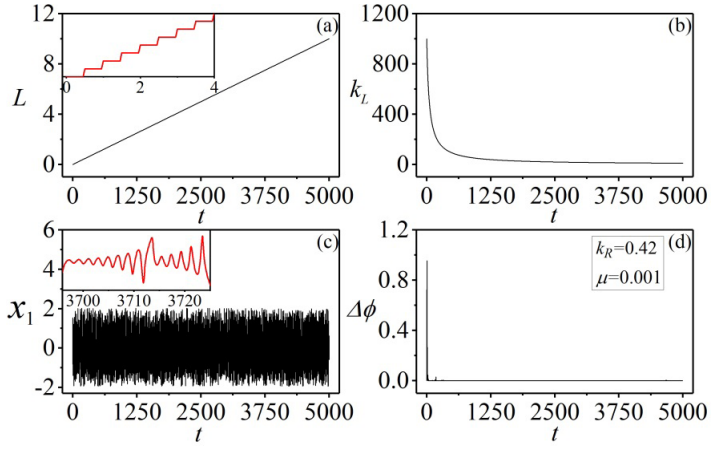

Fig. 12. (Color online) Synchronization approach by using saturation gain method. (a) Increasing the capacitance of coupling capacitor with step function; (b) regulation of the coupling gain; (c) sampled time series for variable x_1 and (d) evolution of phase error under field coupling. $k_R = 0.42$, $\mu_0 = 0.001$, and the coupling devices are connected in series.

the memristive systems are tamed to show periodical oscillation, and the results are shown in Fig. 14.

When higher step increase of inductance for the coupling induction is applied, chaos in the memristive systems is suppressed for presenting the periodical oscillation and phase lock is driven for reaching the phase synchronization. Furthermore, the coupling channel is activated to discuss the case that the coupling devices are connected in parallel, and the results are shown in Figs. 15 and 16.

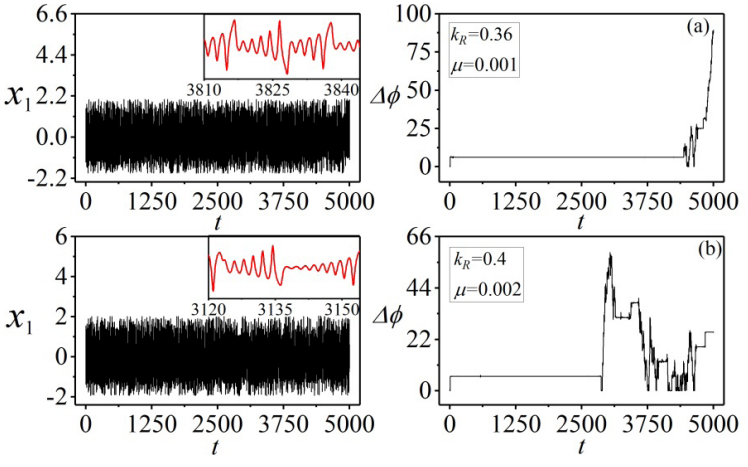

Fig. 13. (Color online) Synchronization approach by using saturation gain method. (a) Sampled time series for variable x_1 and evolution for phase error, $k_R = 0.36$, $\mu_0 = 0.001$ and (b) sampled time series for variable x_1, and evolution for phase error, $k_R = 0.4$, $\mu_0 = 0.002$. The coupling devices are connected in series.

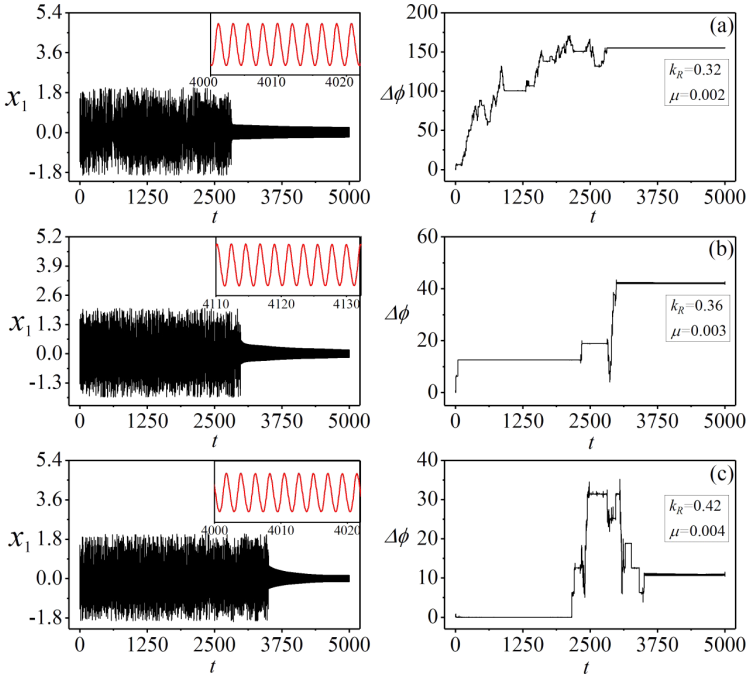

Fig. 14. (Color online) Synchronization approach by using saturation gain method. (a) Sampled time series for variable x_1 and evolution for phase error, $k_R = 0.32$, $\mu_0 = 0.002$; (b) sampled time series for variable x_1, and evolution for phase error, $k_R = 0.36$, $\mu_0 = 0.003$ and (c) sampled time series for variable x_1, and evolution for phase error, $k_R = 0.42$, $\mu_0 = 0.004$. The coupling devices are connected in series.

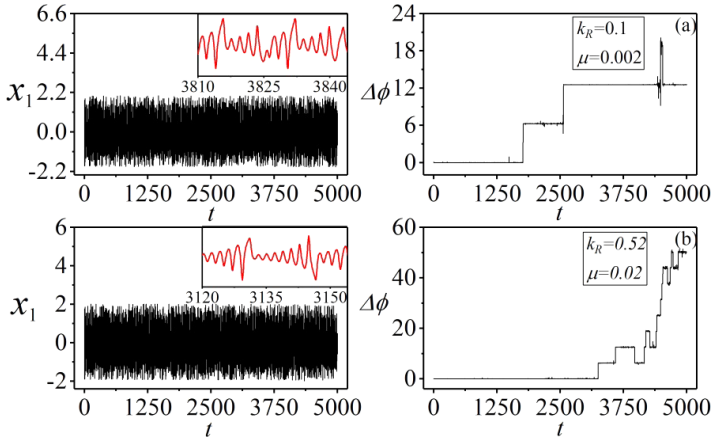

Fig. 15. (Color online) Synchronization approach by using saturation gain method. (a) Sampled time series for variable x_1 and evolution for phase error, $k_R = 0.1$, $\mu_0 = 0.002$ and (b) sampled time series for variable x_1, and evolution for phase error, $k_R = 0.52$, $\mu_0 = 0.02$. The coupling devices are connected in parallel.

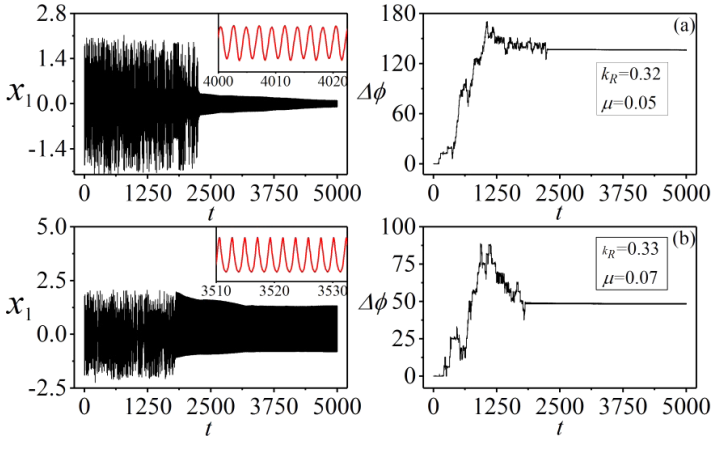

Fig. 16. (Color online) Synchronization approach by using saturation gain method. (a) Sampled time series for variable x_1 and evolution for phase error, $k_R = 0.32$, $\mu_0 = 0.05$ and (b) sampled time series for variable x_1, and evolution for phase error, $k_R = 0.33$, $\mu_0 = 0.07$. The coupling devices are connected in parallel.

From Fig. 15, it demonstrates that intermittent phase lock occurs and the phase error shows distinct step increase when the coupling induction coil is adjusted with the inductance in time. However, the chaos in the coupled memristive systems keeps active even larger coupling intensity is applied. It is interesting to verify whether the chaos in the memristive systems can be suppressed for generating periodical oscillation under phase synchronization, and the results are shown in Fig. 16.

It is confirmed in Fig. 16 that the memristive systems show distinct transition from chaotic oscillation to periodical oscillation, and phase lock is stabilized when the coupling channel is activated. A faster increase of inductance of the coupling induction coil with higher constant step μ_0 can enhance the changes of magnetic flux across the coupling induction coil, and thus energy pumping is regulated to balance the output voltage from the two coupled memristive systems.

Bidirectional coupling provides on effective bridge connection to neurons and nonlinear circuits for feasible signal exchange. When the parameters and nonlinearity are known aforehand, nonlinear analysis can be applied to estimate and select the most appropriate coupling intensity for stabilizing synchronization. In fact, by increasing the coupling intensity with step function, which is called as saturation gain method by adjusting the physical parameter values (capacitance, resistance and inductance) in experimental way, the threshold for coupling synchronization can be detected exactly even when the parameters are unknown. For neurons, this self-adjusting of synapse connection means the activation of synaptic plasticity.

In a summary, resistor, capacitor and induction coil are effective electronic components to bridge connection to nonlinear circuits, and thus coupling channels are built. The involvement of resistor in the coupling channel can introduce energy modulation by consuming Joule heat and thus the output voltage can be balanced for reaching possible synchronization. When capacitor is used to connect the output end of nonlinear circuits, time-varying electric field is induced and field energy is saved by pumping energy from the nonlinear circuits because the output end can charge the plates of the coupling capacitor. On the other hand, time-varying magnetic field is generated in the coupling capacitor which pumps the energy from the coupled circuits. As a result, the energy flow across the coupling channel is injected into the coupling induction coil and induction electromotive force is induced to balance the output voltage for possible synchronization approach. When two different kinds of coupling devices are connected in series, a single coupling channel is built to propagate the same channel current. However, these coupling devices build more than two coupling channels and the channel current is dependent on the contribution from each branch channel.

Confirmed by our scheme, the capacitance of coupling capacitor, inductance of coupling induction coil can be carefully increased with constant step value until the target synchronization is reached. In this way, it seldom needs to know the exact parameters region of the coupled circuits while synchronization approach can be reached.

4. Conclusions

In this paper, resistor, capacitor and induction coil are used to design the artificial hybrid synapses for connecting the memristive circuits, which can be mapped into dimensionless dynamical systems by applying scale transformation on the physical variables and parameters. Considering the self-adaption and synaptic plasticity

of biological neurons, we suggest that the parameters for the coupling devices in the coupling channels can be modulated with self-regulating and thus the coupling intensity can be carefully increased with constant step until synchronization is finalized completely. In this way, this scheme confirms its effectiveness even when the parameters of the memristive systems are unknown. By selecting different step increase and periods, the coupled systems can present distinct transition from chaos to periodicity, also, periodical oscillation can be enhanced to induce chaotic synchronization.

Acknowledgments

This project is supported by the National Natural Science Foundation of China under Grant No. 11672122 and the HongLiu first-class disciplines Development Program of Lanzhou University of Technology.

References

1. E. Kyriakides and J. Georgiou, *Int. J. Circuit Theory Appl.* **43**, 1801 (2015).
2. K. Pyragas and A. Tamaševičius, *Phys. Lett. A* **180**, 99 (1993).
3. B. R. Andrievskii and A. L. Fradkov, *Autom. Remote Control* **64**, 673 (2003).
4. C. Li *et al.*, *IEEE MultiMedia* **25**, 46 (2018).
5. C. Li *et al.*, *IEEE Access* **6**, 75834 (2018).
6. Q. Gan *et al.*, *Int. J. Circuit Theory Appl.* **45**, 1849 (2017).
7. X. Han, B. Jiang and Q. Bi, *Nonlinear Dyn.* **61**, 667 (2010).
8. X. Han *et al.*, *Phys. Rev. E* **92**, 012911 (2015).
9. X. Han *et al.*, *Chaos* **28**, 043111 (2018).
10. Y. Yu *et al.*, *Commun. Nonlinear Sci. Numer. Simul.* **47**, 23 (2017).
11. M. Storace, D. Linaro and E. de Lange, *Chaos* **18**, 033128 (2008).
12. Z. Zhao, L. Li and H. Gu, *Front. Cell. Neurosci.* **12**, 62 (2018).
13. Z. Zhao and H. Gu, *Sci. Rep.* **7**, 6760 (2017).
14. L. L. Lu *et al.*, *Sci. China Technol. Sci.* **62**, 427 (2019).
15. C. Wang and J. Ma, *Int. J. Mod. Phys. B* **32**, 1830003 (2018).
16. M. Ge *et al.*, *Appl. Math. Comput.* **352**, 136 (2019).
17. Y. Xu *et al.*, *Neurocomputing* **283**, 196 (2018).
18. G. Zhang *et al.*, *Commun. Nonlinear Sci. Numer. Simul.* **65**, 79 (2018).
19. H. Qin *et al.*, *Physica A* **501**, 141 (2018).
20. S. Rakshit *et al.*, *Phys. Rev. E* **100**, 012315 (2019).
21. S. Majhi *et al.*, *Phys. Life Rev.* **28**, 100 (2019).
22. M. Shafiei *et al.*, *Eur. Phys. J. B* **92**, 36 (2019).
23. F. Parastesh *et al.*, *Appl. Math. Comput.* **350**, 217 (2019).
24. C. Wang *et al.*, *Chaos* **27**, 113108 (2017).
25. Y. Xu *et al.*, *Neurocomputing* **207**, 398 (2016).
26. L. Xiang and J. J. H. Zhu, *Nonlinear Dyn.* **64**, 339 (2011).
27. A. Stožer *et al.*, *Front. Physiol.* **10**, 869 (2019).
28. Z. Rostami *et al.*, *Physica A* **509**, 1162 (2018).
29. L. Lu *et al.*, *Nonlinear Dyn.* **95**, 1673 (2019).
30. J. Ma *et al.*, *Neurocomputing* **167**, 378 (2015).
31. J. Ma *et al.*, *Physica A* **536**, 122598 (2019).

32. C. N. Wang, J. Tang and J. Ma, *Eur. Phys. J. Spec. Top.* **228**, 1907 (2019).
33. B. Rörig and B. Sutor, *Mol. Neurobiol.* **12**, 225 (1996).
34. R. Dermietzel and D. C. Spray, *Trends Neurosci.* **16**, 186 (1993).
35. R. Rozental, C. Giaume and D. C. Spray, *Brain Res. Rev.* **32**, 11 (2000).
36. N. Burić, K. Todorović and N. Vasović, *Phys. Rev. E* **78**, 036211 (2008).
37. N. Kopell and B. Ermentrout, *Proc. Nat. Acad. Sci.* **101**, 15482 (2004).
38. S. Mostaghimi *et al.*, *Appl. Math. Comput.* **348**, 42 (2019).
39. J. Ma *et al.*, *J. Zhejiang Univ.-Sci. A* **20**, 639 (2019).
40. Z. Liu *et al.*, *Appl. Math. Comput.* **360**, 94 (2019).
41. Y. Xu *et al.*, *Front. Inf. Technol. Electron. Eng.* **20**, 571 (2019).
42. S. Ma *et al.*, *AEU-Int. J. Electron. Commun.* **105**, 177 (2019).
43. D. Yu *et al.*, *IEEE Access* **5**, 1284 (2017).
44. Z. Yao *et al.*, *Nonlinear Dyn.* **96**, 205 (2019).
45. J. Ma *et al.*, *Nonlinear Dyn.* **93**, 2057 (2018).
46. Z. Liu *et al.*, *Int. J. Mod. Phys. B* **32**, 1950170 (2019).
47. J. Valsa, D. Biolek and Z. Biolek, *Int. J. Numer. Model. Electron. Netw. Devices Fields* **24**, 400 (2011).
48. M. Itoh and L. O. Chua, *Int. J. Bifurcation Chaos* **18**, 3183 (2008).
49. F. Corinto, A. Ascoli and M. Gilli, *IEEE Trans. Circuits Syst. I* **58**, 1323 (2011).
50. H. Bao *et al.*, *IEEE Trans. Neural Netw. Learn. Syst.* **31**(2), 502 (2020).
51. Y. Zhang *et al.*, *IEEE Access* **7**, 109689 (2019).
52. L. Chen *et al.*, *Nonlinear Dyn.* **98**, 517 (2019).
53. I. Boybat *et al.*, *Nat. Commun.* **9**, 2514 (2018).
54. F. Wu, J. Ma and G. Ren, *J. Zhejiang Univ. Sci. A* **19**, 889 (2018).
55. H. G. Wu *et al.*, *Chaos Solitons Fractals* **121**, 178 (2019).
56. Y. Liu *et al.*, *Physica A* **520**, 370 (2019).
57. H. Gu, B. Pan and Y. Li, *Nonlinear Dyn.* **82**, 1191 (2015).
58. B. Muthuswamy and L. O. Chua, *Int. J. Bifurcation Chaos* **20**, 1567 (2010).
59. L. O. Chua and G. N. Lin, *IEEE Trans. Circuits Syst.* **37**, 885 (1990).
60. L. O. Chua, *J. Circuits, Syst. Comput.* **4**, 117 (1994).